Nanoscale

MINIREVIEW

View Article Online
View Journal | View Issue

Cite this: *Nanoscale*, 2023, **15**, 6521

Alternatives to water oxidation in the photocatalytic water splitting reaction for solar hydrogen production

Yaqiang Wu,[a] Takuya Sakurai,[a] Takumi Adachi[a] and Qian Wang *[a,b]

Received 17th January 2023,
Accepted 4th March 2023

DOI: 10.1039/d3nr00260h

rsc.li/nanoscale

The photocatalytic water splitting process to produce H_2 is an attractive approach to meet energy demands while achieving carbon emission reduction targets. However, none of the current photocatalytic devices meets the criteria for practical sustainable H_2 production due to their insufficient efficiency and the resulting high H_2 cost. Economic viability may be achieved by simultaneously producing more valuable products than O_2 or integrating with reforming processes of real waste streams, such as plastic and food waste. Research over the past decade has begun to investigate the possibility of replacing water oxidation with more kinetically and thermodynamically facile oxidation reactions. We summarize how various alternative photo-oxidation reactions can be combined with proton reduction in photocatalysis to achieve chemical valorization with concurrent H_2 production. By examining the current advantages and challenges of these oxidation reactions, we intend to demonstrate that these technologies would contribute to providing H_2 energy, while also producing high-value chemicals for a sustainable chemical industry and eliminating waste.

As humanity moves forward into the 21st century, the supplementation of clean and sustainable energy is one of our greatest scientific and technical challenges. The photocatalytic water splitting process using nanoparticulate photocatalysts and solar energy is a leading candidate to achieve low-carbon production of H_2 as a clean and sustainable energy carrier. In this process, water is split into H_2 and O_2 *via* the following redox reactions (eqn (1) and (2); pH 0 in aqueous solution *versus* (normal hydrogen electrode) NHE, 25 °C, 1 atm gas pressure, and 1 M for other solutes):

$$2H^+ + 2e^- \rightarrow H_2 \quad E^\circ = 0\ \text{V} \tag{1}$$

$$2H_2O \rightarrow O_2 + 4H^+ + 4e^- \quad E^\circ = +1.23\ \text{V} \tag{2}$$

Water splitting is a non-spontaneous chemical reaction involving water oxidation to O_2, which requires four electrons to simultaneously transfer from at least two water molecules. Photocatalysis is a light-driven chemical process that involves oxidation and reduction reactions by the photogenerated electrons and holes. To achieve the photocatalytic water splitting reaction, the conduction band minimum must be more negative than the H^+ to H_2 reduction potential, while the valence band maximum must be more positive than the H_2O to O_2 oxidation potential. Consequently, the minimum theoretical energy required to initiate the water-splitting reaction is 1.23 eV. However, O_2 evolution from water leads to sluggish kinetics and high additional kinetic overpotentials,[1,2] making photocatalytic H_2 evolution need the use of sacrificial reagents to provide an electron source.[3–5] Specifically, the overpotential losses of the oxygen evolution reaction (OER) can reach up to 30%, resulting in a significant amount of wasted energy.[6] In addition, the lack of effective methods to separate the produced O_2 and H_2 gases is a key problem for the practical application of photocatalytic water splitting.[7] As a result of these challenges, increasing attention is being focused on emerging replacements for the OER that may support an expanding H_2 economy globally.

In this minireview, we highlight a variety of key reactions that are well suited as potential replacements for the OER, focusing on the recent developments in the study of photoreforming and photochemical oxidation reactions to produce value-added organic and inorganic products that have received considerable attention in the literature, such as formic acid (~1.1 $ per kg) production from waste PET (≤0 $ per kg) and H_2O_2 (~0.7 $ per kg) formation by water (~2.9×10^{-4} $ per kg) oxidation.[8,9] These reactions are appealing because they would enable (1) the production of more valuable chemicals than O_2 (~0.1 $ per kg) alongside the production of H_2; (2) the elimin-

---

[a] *Graduate School of Engineering, Nagoya University, Furo-cho, Chikusa-ku, Nagoya 464-8603, Japan. E-mail: wang.qian@material.nagoya-u.ac.jp; Tel: +81-527893250*

[b] *Institute for Advanced Research, Nagoya University, Furo-cho, Chikusa-ku, Nagoya 464-8601, Japan*

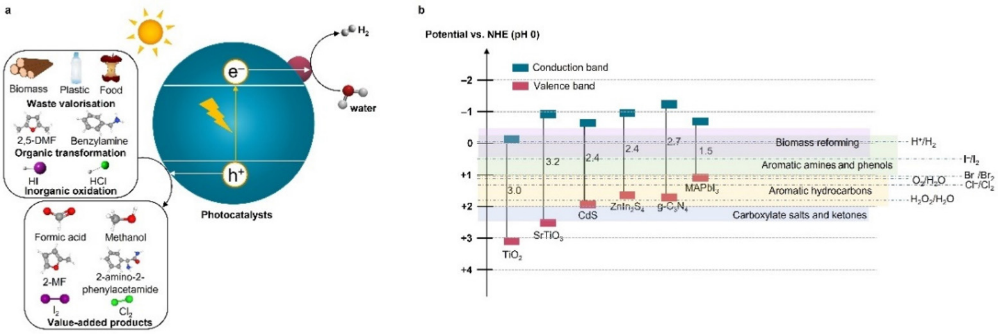

Fig. 1 (a) Diagram of the photooxidation reactions rather than water-to-O_2 oxidation combing with solar H_2 production. (b) Band structures of representative photocatalysts and standard redox potentials for some common oxidation reactions. Data were obtained from ref. 6.

ation of the need for a H_2 and O_2 mixture separation unit, thereby lowering the cost, improving the safety, and simplifying the design of photocatalytic processes; and (3) reduced overpotential due to the simper 1 or 2 electron net oxidation mechanisms, which would result in an increased conversion efficiency and reaction rate.[6] Under light irradiation, an inorganic or organic substrate is oxidized by the photoexcited holes at the valence band, which subsequently generated valuable chemicals or CO_2 or intermediate products and protons (Fig. 1a). The protons are reduced by electrons at the conduction band to produce H_2. While the direct oxidation of alternative substrates combined with the production of clean H_2 can be feasibly carried out using various technologies including electrolysis, photoelectrochemical and photocatalytic systems,[6,7,10] we have targeted cases that have been demonstrated using nanoparticulate photocatalysts due to their potential for large-scale operations.

Qian Wang

Qian Wang is currently an Associate Professor at Nagoya University, Japan. She received her Ph.D. in 2014 from the University of Tokyo, Japan and then worked as a postdoctoral researcher for the Japan Technological Research Association of Artificial Photosynthetic Chemical Processes (ARPChem) project at the University of Tokyo. In 2018, she became a Marie Sklodowska-Curie Research Fellow at the University of Cambridge. She joined Nagoya University as an Associate Professor in May 2021 and established her research group, which is currently developing new materials, approaches, and technologies for solar energy storage in the form of renewable fuels via *artificial photosynthesis.*

Photoreforming

Photocatalytic reforming that harnesses solar energy to convert sustainable or waste feedstocks for H_2 generation has become one of the most rapidly evolving applications in the field due to its ability to valorize a range of feedstocks especially biomass, food and plastics (≤0 $ per kg) to both energy and value-added products (such as formic acid (~1.1 $ per kg), methanol (~0.6 $ per kg), acetaldehyde (~2 $ per kg) and lactic acid (~3 $ per kg)), as listed in Table 1.[9] Research trends highlight the shift from the early work which focused on simple model substrates such as ethanol, glycerol, and cellulose to more recent work that utilizes real waste, making the process more complex but more economically and environmentally sustainable.[11] The energetics of coupling the oxidation of a variety of common organic waste substrates with H_2 evolution are nearly neutral (Fig. 1b), for example, glucose oxidation (eqn (3)), making it more favorable than water splitting, although these oxidation reactions involve multiple electron transfer steps.[12] Theoretically, coupling photoreforming with H_2 production would no longer restrict the use of semiconductors with deep valence bands, allowing the application of those with a smaller bandgap. The photocatalytic reforming could therefore be driven by a large portion of incident sunlight including visible and IR parts.

$$\begin{aligned} &C_6H_{12}O_6 + 6H_2O \rightarrow 6CO_2 + 24H^+ + 24e^- \\ &E^\circ = -0.001\,\mathrm{V}\ vs.\ \mathrm{NHE} \end{aligned} \tag{3}$$

$$C_xH_yO_z + (2x - z)H_2O \xrightarrow{h\nu} xCO_2 + \left(2x - z + \frac{y}{2}\right)H_2 \tag{4}$$

Initially, photocatalytic reforming research centered on the production of H_2 from a variety of lignocellulose biomass-derived feedstocks, the most abundant and non-edible biomass resource, including monosaccharides, such as pentoses (ribose and arabinose) and hexoses (glucose, fructose, galactose, and mannose), alcohols (methanol, propanol, ethanol, and butanol) and organic acids (formic acid and acetic acid).[12–19] Theoretically, in the proposed biomass photoreforming process, photoexcited holes lead to the oxidation of biomass components and derivatives (denoted as $C_xH_yO_z$),

Table 1 Performance metrics for some recent representative solar fuel production systems using alternative photooxidation reactions to the OER

Substrates	Photocatalysts	Reaction conditions	Products	Efficiency	Reaction time	Ref.
Glucose	Pt/C_3N_4 (~ 1 μm)	40 W blue LED (λ = 427 nm) 10 M KOH	H_2: 3.39 mmol g^{-1} h^{-1} Lactic acid	Glucose conversion: 100% Selectivity (lactic acid): 86%	16 hours	28
Microcrystalline cellulose	Pt/TiO_2	16 W UV-A lamp (λ = 365 nm)	H_2: 13.3 μmol h^{-1}	QE: 42.8% at 365 nm	5 hours	25
Cellulose	Pt/S- and N-doped graphene oxide dots (2–7 nm)	Simulated sunlight (AM 1.5G, 100 mW cm^{-2}) pH 12.5	H_2: 100 μmol h^{-1} Acetaldehyde, methanol, formate, *etc.*	QE: 23.3% at 420 nm	6 days	108
Glucose	TiO_2/Co(terpyridine)$_2$ (~20 nm)	Simulated sunlight (AM 1.5G, 100 mW cm^{-2}) Aqueous sodium acetate and MeCN purged with CO_2	H_2: ~0.43 mmol per $g_{catalyst}$ per 24 h CO: ~0.43 mmol per $g_{catalyst}$ per 24 h Formate: ~1.18 mmol per $g_{catalyst}$ per 24 h	Glucose conversion efficiency: 20% QE: 0.22–0.41% at 360 nm for CO; 1.05–1.45% at 360 nm for formate	24 hours	48
Cellobiose	TiO_2/Co(terpyridine)$_2$ (~20 nm)	Simulated sunlight (AM 1.5G, 100 mW cm^{-2}) Aqueous sodium acetate and MeCN purged with CO_2	H_2: ~0.72 mmol per $g_{catalyst}$ per 24 h CO: ~0.92 mmol per $g_{catalyst}$ per 24 h Formate: ~1.03 mmol per $g_{catalyst}$ per 24 h	Cellobiose conversion efficiency: 8.6%	24 hours	48
Glycerol	Cu/TiO_2 nanorods	LED irradiation (λ = 365 nm) MeCN–water solution	H_2: 22 mmol per $g_{catalyst}$ per 12 h Methanol, CO, and CO_2	QE: 3.4% at 365 nm	12 hours	49
Cellulose	Pt/$^{NCN}CN_x$	Simulated sunlight (AM 1.5G, 100 mW cm^{-2}) LiBr and LiOH in 0.1 M H_2SO_4 solution	H_2: ~190 mmol $g_{catalyst}^{-1}$ h^{-1} Formic acid, lactic acid, arabinose, erythrose, *etc.*		24 hours	50
Cellulose	**NiP**/carbon dots (<10 nm)	Simulated sunlight (AM 1.5G, 100 mW cm^{-2})	H_2: ~5 μmol per 24 h $C_6H_{12}O_6$ and $C_6H_{10}O_5$ compounds		24 hours	26
Glucose	**NiP**/carbon dots (<10 nm)	Simulated sunlight (AM 1.5G, 100 mW cm^{-2})	H_2: ~6 μmol per 24 h $C_6H_{12}O_6$ and $C_6H_{10}O_5$ compounds		24 hours	26
Cellulose	Pt/P25 TiO_2 (20–30 nm)	UV–vis light (250 W iron doped halide lamp) 0.6 M H_2SO_4 solution 403 K; 3.0 bar	H_2: ~170 μmol per 10 h HMF, erythrose, and arabinose		10 hours	35
α-Cellulose	CdS/CdO_x quantum dots (diameter ~5 nm)	Simulated sunlight (AM 1.5G, 100 mW cm^{-2}) 10 M KOH	H_2: ~2.57 mmol $g_{catalyst}^{-1}$ h^{-1} Formate, carboxylic acid, CO_2, *etc.*		6 days	24
Fructose	CdS/CdO_x quantum dots	Simulated sunlight (AM 1.5G, 100 mW cm^{-2}) 10 M KOH	H_2: ~1070 mmol per $g_{substrate}$ per 20 h Formate, *etc.*	QE: 2.73% at 430 nm	20 hours	45
Starch	CdS/CdO_x quantum dots	Simulated sunlight (AM 1.5G, 100 mW cm^{-2}) 10 M KOH	H_2: ~462 mmol per $g_{substrate}$ per 20 h Formate, *etc.*		20 hours	45
Apple	CdS/CdO_x quantum dots	Simulated sunlight (AM 1.5G, 100 mW cm^{-2}) 10 M KOH	H_2: ~6070 mmol $g_{catalyst}^{-1}$ h^{-1}		20 hours	45
Cheese	CdS/CdO_x quantum dots	Simulated sunlight (AM 1.5G, 100 mW cm^{-2}) 10 M KOH	H_2: ~9350 mmol $g_{catalyst}^{-1}$ h^{-1}		20 hours	45
Artificial mixed waste	CdS/CdO_x quantum dots	Simulated sunlight (AM 1.5G, 100 mW cm^{-2}) 10 M KOH	H_2: ~9900 mmol $g_{catalyst}^{-1}$ h^{-1}		20 hours	45
Municipal waste	CdS/CdO_x quantum dots	Simulated sunlight (AM 1.5G, 100 mW cm^{-2}) 10 M KOH	H_2: ~5920 mmol $g_{catalyst}^{-1}$ h^{-1}		20 hours	45
Wooden branch	CdS/CdO_x quantum dots (diameter ~5 nm)	Simulated sunlight (AM 1.5G, 100 mW cm^{-2}) 10 M KOH	H_2: ~5.59 mmol $g_{catalyst}^{-1}$ h^{-1}		24 hours	24
Municipal solid waste	CN_x/$\mathbf{Ni_2P}$	Simulated sunlight (100 mW cm^{-2}) 0.5 M KOH	Formate, carbonate, *etc.* H_2: 130 mmol h^{-1} m^{-2}		20 hours	39
PLA	CdS/CdO_x quantum dots (diameter ~5 nm)	Simulated sunlight (AM 1.5G, 100 mW cm^{-2}) 10 M NaOH	H_2: ~64.3 mmol $g_{catalyst}^{-1}$ h^{-1} Pyruvate, *etc.*	QE: 15.0% at 430 nm	4 hours	37

Table 1 *(Contd.)*

Substrates	Photocatalysts	Reaction conditions	Products	Efficiency	Reaction time	Ref.
PET	CdS/CdO_x quantum dots (diameter ~5 nm)	Simulated sunlight (AM 1.5G, 100 mW cm^{-2}) 10 M NaOH	H_2: ~3.42 mmol $g_{catalyst}^{-1}$ h^{-1} Formate, glycolate, ethanol, acetate, and lactate	QE: 3.74% at 430 nm	4 hours	37
PUR	CdS/CdO_x quantum dots (diameter ~5 nm)	Simulated sunlight (AM 1.5G, 100 mW cm^{-2}) 10 M NaOH	H_2: ~0.85 mmol $g_{catalyst}^{-1}$ h^{-1} Formate, acetate, pyruvate, and lactate	QE: 0.14% at 430 nm	4 hours	37
PET water bottle	CdS/CdO_x quantum dots(diameter ~5 nm)	Simulated sunlight (AM 1.5G, 100 mW cm^{-2}) 10 M NaOH	H_2: ~4.13 mmol $g_{catalyst}^{-1}$ h^{-1} Formate, glycolate, ethanol, acetate, lactate, glyoxylate, methylglyoxal, and methanol	QE: 2.17% at 430 nm Conversion: 5.15%	24 hours	37
Methanol	$CoP/Zn_2In_2S_5$ nanosheets	Simulated sunlight (AM 1.5G)	H_2: ~21 mmol $g_{catalyst}^{-1}$ h^{-1} Ethylene glycol: 18.9 mmol $g_{catalyst}^{-1}$ h^{-1} HCHO: ~4 mmol $g_{catalyst}^{-1}$ h^{-1}		12 hours	67
Ethanol	$CoP/Zn_2In_2S_5$ nanosheets	300 W Xe lamp (λ = 400–780 nm)	H_2: ~8.5 mmol $g_{catalyst}^{-1}$ h^{-1} 2,3-Butanediol: 3.2 mmol $g_{catalyst}^{-1}$ h^{-1} CH_3CHO: ~5 mmol $g_{catalyst}^{-1}$ h^{-1}		12 hours	67
Benzyl alcohol	$Zn_{0.2}In_2S_{3.2}$	6 W LED (λ = 365 ± 5 nm)	H_2 yield: 172% Benzoin yield: 61% Deoxybenzoin yield: 30% Benzaldehyde yield: 9%		12 hours	58
Furfural alcohol	$Ti_3C_2T_x/CdS$ nanosheets (~60 nm)	300 W Xe lamp ($\lambda \geq$ 420 nm)	H_2: 773 µmol per $g_{catalyst}$ per 4 h Furfural: 777 µmol per $g_{catalyst}$ per 4 h		4 hours	54
Cetophenone	Pd/TiO_2	6 W LED (λ = 365 ± 5 nm) Ethanol	H_2: ~0.25 mmol per 3 h Phenethanol: ~0.55 mmol per 3 h Ethylbenzene: ~0.05 mmol pre 3 h Acetaldehyde: ~0.4 mmol per 3 h		3 hours	109
DMF	Ni/CdS nanosheets	300 W Xe lamp ($\lambda \geq$ 420 nm)	H_2: ~1 mmol per 3 h *N*-Benzylidenebenzylamine: ~2 mmol per 5 h	QE: ~44% at 420 nm	3 hours	69
Benzyl alcohol	$Zn_3In_2S_6$ (1–3 µm)	300 W Xe lamp (λ > 380 nm)	H_2: 708.8 µmol per 4 h Benzaldehyde: 732 µmol per 4 h	QE: 6.48% at 380 nm 5.46% at 400 nm 4.02% at 420 nm 1.03% at 450 nm	4 hours	64
DMA	Pt/CN_x	14.4 W blue LED (λ_{max} = 470 nm)	H_2: ~12 µmol per 10 h Minisci oxidation products: ~15 µmol per 10 h		10 hours	59
THF	Pt/CN_x	14.4 W blue LED (λ_{max} = 470 nm)	H_2: ~9 µmol per 10 h Minisci oxidation products: ~9.5 µmol per 10 h		10 hours	59
2,5-DMF	$Ru–ZnIn_2S_4$ (0.6–1.6 µm)	9 W blue LED (λ = 455 nm)	H_2: ~6.0 mmol $g_{catalyst}^{-1}$ h^{-1} DFPs: ~1.04 g $g_{catalyst}^{-1}$ h^{-1}	QE: 15.2% at 452 nm	6 hours	68
2-MF	$Ru–ZnIn_2S_4$ (0.6–1.6 µm)	9 W blue LED (λ = 455 nm)	H_2: ~1.2 mmol $g_{catalyst}^{-1}$ h^{-1} DFPs: ~0.1 g $g_{catalyst}^{-1}$ h^{-1}	QE: 1.9% at 452 nm	12 hours	68
HMF	Pt/porous carbon nitride	Simulated sunlight (λ > 400 nm, 100 mW cm^{-2})	H_2: 12 µmol m^{-2} h^{-1} DFF: 1.3µmol m^{-2} h^{-1}	DFF yield: 13.8% after 6 h Selectivity >99%	6 hours	53
Benzylamine	Ni/CdS nanoparticles	1.85 W Xe lamp (λ > 420 nm)	H_2: 21.4 mmol $g_{catalyst}^{-1}$ h^{-1} Imine	Conversion: 99% Selectivity for imine: 97% QE: 11.2% at 450 nm	45 minutes	60
Benzyl mercaptane	$PtS/ZnIn_2S_4$ nanocomposites	5 W LED (λ = 450 nm)	H_2 yield: 100% Dibenzyl disulfide	Conversion: ~100% after 6 h Selectivity of dibenzyl disulfide: ~100% QE: 24.96% at 420 nm	6 hours	61
Methanol	MoS_2 foam/CdS nanorods	300 W Xe lamp (λ = 420–780 nm)	H_2: 12 mmol $g_{catalyst}^{-1}$ h^{-1} Ethylene glycol, *etc.*		12 hours	66
MBA	**RuCat**/Pt–g-C_3N_4	300 W Xe lamp (λ > 400 nm)	H_2: 56 µmol per 10 h MBAd	QE: 0.28% at 400 nm	10 hours	65
Furfural alcohol	Ni/CdS nanosheets (thickness ~1 nm)	8 W blue LED (λ = 450 nm)	H_2: ~5 mL per 8 h Furfural		8 hours	52
HMF	Ni/CdS nanosheets (thickness ~1 nm)	8 W blue LED (λ = 450 nm)	H_2: ~0.5 mL per 8 h DFF		8 hours	52
4-MBA	**NiP**/$^{NCN}CN_x$	Simulated sunlight (AM 1.5G, 100 mW cm^{-2})	H_2: ~21.3 µmol per 24 h 4-MBAd: ~19.8 µmol per 24 h	QE: 15% at 360 nm	24 hours	57
H_2O	$CdS-ZnIn_2S_4$ nanosheets	300 W Xe lamp (λ > 400 nm)	H_2: ~0.5 mmol $g_{catalyst}^{-1}$ h^{-1} H_2O_2: ~0.6 mmol $g_{catalyst}^{-1}$ h^{-1}	QE: 1.63% at 400 nm	12 hours	86
HI	$MoS_2/MAPbI_3$	280 W Xe lamp ($\lambda \geq$ 420 nm)	H_2: ~29.4 mmol $g_{catalyst}^{-1}$ h^{-1} I_3^-	QE: 13–22% in the range of 420–850 nm STH: 7.35%	90 hours	102

accompanied by hydrogen generation through the reduction of protons by electrons (eqn (4)). The irreversible reaction of $C_xH_yO_z$ with photogenerated holes results in the concomitant suppression of electron–hole recombination and back reactions involving the produced H_2, thereby increasing the quantum efficiency and the rate of H_2 evolution.[13]

Nevertheless, lignocellulose refining is costly and inefficient, typically necessitating acid hydrolysis, enzymatic hydrolysis, or pyrolysis to produce more manageable substrates.[20] Therefore, viable H_2 production systems should directly reform lignocellulose. The main components of lignocellulosic biomass are cellulose (35–50%), hemicellulose (25–30%), and lignin (15–30%).[21,22] Cellulose,[23–28] hemicellulose[24,29,30] and lignin[24,26,31,32] have been reported to produce H_2 using various photocatalysts such as TiO_2, CdS/CdO_x quantum dots, carbon dots, carbon nitride, and CdS (Table 1). Metallic nanoparticulate cocatalysts (*e.g.*, Pt, Au, and Pd) and non-precious cocatalysts (*e.g.*, NiP and NiS) are frequently loaded on photosensitizers by wet impregnation and photodeposition methods, with Pt the most commonly studied.[33] As an example, CdS/CdO_x quantum dots loaded Co species as cocatalysts were reported to perform photoreforming of cellulose, hemicellulose and lignin to H_2 in alkaline solution under simulated sunlight irradiation (H_2 evolution rates for cellulose, hemicellulose, and lignin were 2.57, 2.32, and 0.53 mmol $g_{catalyst}^{-1}$ h^{-1}, respectively).[24]

Reports on using raw biomass as the substrate for photoreforming are limited. Although direct H_2 production from unprocessed biomass has the advantage of lower production costs, it is limited by low substrate solubility. Additionally, light is scattered and absorbed by insoluble biomass and colored components, lowing the light absorption efficiency. The recalcitrance of raw biomass may lead to a large overpotential for biomass oxidation.[12] TiO_2 is frequently used as a photocatalyst for raw biomass reforming, despite its large bandgap (around 3.2 eV) and limited sunlight utilization ability. The H_2 evolution rates of TiO_2 for the photoreforming of raw biomass, such as poplar wood chips,[27] rice husk,[34] paper pulp,[35] chlorella algae,[36] and turf,[36] are in the range of 0.01–0.1 mmol $g_{catalyst}^{-1}$ h^{-1}, which are typically lower than those obtained using carbon nitride and CdS with narrower bandgaps (carbon nitride: ~2.7 eV; CdS: ~2.4 eV) (Table 1).[24,29] For instance, a rate of over 5 mmol H_2 $g_{catalyst}^{-1}$ h^{-1} was reported through photoreforming a wooden branch on Co/CdS/CdO_x, as shown in Fig. 2. The system was stable for more than 6 days and was capable of reforming unprocessed lignocellulose, demonstrating a cost-effective approach to produce H_2 from waste biomass. The high H_2 evolution rate may also be attributed to the alkaline conditions that not only provide an *in situ* pretreatment of lignocellulose by dissolving hemicellulose, lignin, cellulose, and other saccharides but also facilitate CdO_x deposition on CdS, thereby producing a photocatalyst that is active and resistant to corrosion.[24]

The ideal feedstock for photoreforming comes from waste streams that cannot be recycled or reused in any other way.[11] To this end, the photooxidation of food waste and nonrecycled plastics has recently become an emerging topic in the field.[11,37–44] The chemical composition of food waste varies greatly. Due to their hydrophobicity and typically chemically inert hydrocarbon chain, photoreforming fats in an aqueous solution is more difficult than photoreforming proteins composed of long chains of amino acid residues (Table 1).[11] Under simulated solar irradiation, simultaneous production of H_2 and the oxidation of a variety of carbohydrates, proteins and fats as well as real-world waste (apples, bread, and cheese) to generate formate and CO_2 or carbonate was observed over CdS/CdO_x quantum dots and Ni_2P/CN_x.[45] The carbon footprints of these processes were estimated to be 44 600–68 800 g_{CO2} per kWh H_2 with a conversion efficiency of 1.9–22% after 3 days, which were still high due to the need for alkaline solutions as well as energy for stirring, and pre-treatment (accounts for more than 90% of the values).[45] The carbon footprint can be reduced to a negative value of −3200 g_{CO2} per kWh H_2 if the waste in the water is 100% converted to H_2 and formate.

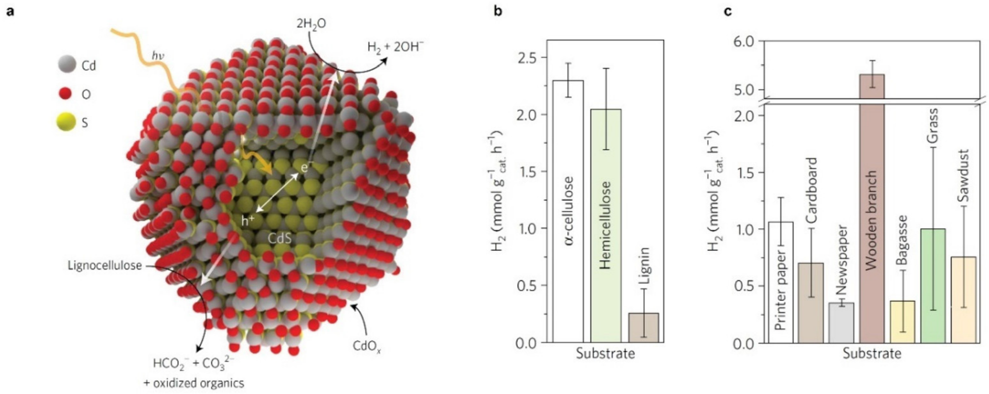

Fig. 2 (a) Diagram of the photoreforming of lignocellulose to H_2 on CdS/CdO_x. (b and c) Photocatalytic production rates of H_2 from α-cellulose, hemicellulose and lignin (b), and raw and waste biomass substrates (c) using Co/CdS/CdO_x quantum dots in 10 M KOH aqueous solution under simulated solar light (AM 1.5G, 100 mW cm^{-2}). Reproduced with permission from ref. 24. Copyright 2017 Macmillan Publishers Limited, part of Springer Nature.

Therefore, improvements in the conversion efficiency and photooxidation process selectivity are required.

In comparison with the photodegradation of plastics that converts plastics into CO_2 and H_2O, photorefoming can not only reduce plastic pollution but also produce fuels and products with added value, including pyruvate (~190 \$ per kg), glycolate (~450 \$ per kg), formic acid (~1.1 \$ per kg), ethanol (~1.2 \$ per kg) and acetic acid (~1.2 \$ per kg) (Table 1),[9] allowing for a substantial economic advantage and a higher atom economy. While hydrocarbon chains such as polyethylene (PE), polystyrene (PS), and polypropylene (PP) in plastics are currently difficult to reform due to their highly stable C–C bonds, the oxygen-containing esters including polyethylene terephthalate (PET) (eqn (5) and (6)), polylactic acid (PLA) (eqn (7) and (8)) and polyurethane (PUR) (eqn (9) and (10)) can facilitate photoreforming after proper hydrolysis treatment.[37]

$$\text{PET}: C_{10}H_8O_4+2H_2O \overset{\text{NaOH}}{\longrightarrow} C_8H_6O_4+C_2H_6O_2 \tag{5}$$

$$C_2H_6O_2+2H_2O \xrightarrow[\text{Photocatalyst}]{hv} 2CO_2+5H_2 \tag{6}$$

$$\text{PLA}: C_3H_4O_2+H_2O \overset{\text{NaOH}}{\longrightarrow} C_3H_6O_3 \tag{7}$$

$$C_3H_6O_3+3H_2O \xrightarrow[\text{Photocatalyst}]{hv} 3CO_2+6H_2 \tag{8}$$

$$\begin{aligned}&\text{PUR}: C_{12}H_{14}N_2O_4+2H_2O \overset{\text{NaOH}}{\longrightarrow} C_7H_{10}N_2\\&+C_3H_8O_2+2CO_2\end{aligned} \tag{9}$$

$$C_3H_8O_2+4H_2O \xrightarrow[\text{Photocatalyst}]{hv} 3CO_2+8H_2 \tag{10}$$

The reforming of plastics conjugating with proton reduction to H_2 is also nearly energy neutral.[40] For instance, the Gibbs free energy changes for the reforming of ethylene glycol (a monomer of PET) and lactic acid (a monomer of PLA) are +9.2 kJ mol^{-1} and +27 kJ mol^{-1}, respectively. A variety of plastics including PLA, PET, PUR, and a PET water bottle were oxidized by photogenerated holes in CdS/CdO_x quantum dots into a range of substrate-dependent organic products (*e.g.*, formate, glycolate, ethanol, acetate, and pyruvate) in 10 M NaOH aqueous solution, while the photogenerated electrons reduced protons to produce H_2 with a rate of 3–65 mmol $g_{catalyst}^{-1}$ h^{-1} (Table 1, and Fig. 3).[37] A Ni_2P/CN_x photocatalyst which is inexpensive and nontoxic has also shown promising activities for visible-light-driven PET and PLA reforming to produce H_2 fuel and a variety of organic chemicals under alkaline aqueous conditions.[46] The challenge in plastic photoreforming is the competition with plastic dehydrogenation to H_2 and selective oxidation to a single product rather than CO_2.[47] The reported conversion of plastics was up to 30%–40%, which requires further improvement. Furthermore, these studies imply that photoreactions can cleave C–C, C–N, and C–O bonds in the aliphatic chains of plastics as effectively as hydrolysis.

It is suggested that a theoretical maximum of 310–650 Mt of H_2 could be produced each year (the equivalent of ~6–13% of annual global energy consumption) if the above biomass, food and plastic components were all utilized for photoreforming.[11] The preliminary techno-economic and life cycle assessment of photoreforming has shown that it has a lower carbon footprint than or is comparable to existing methods for producing H_2, converting waste to fuel, and managing waste, but the improvement in production costs and energy balance is still required before industrial applications can be envisaged. Although the product of the oxidation reaction in photoreforming is typically CO_2, it is preferred that valuable organic chemicals can be produced instead of CO_2 to improve the sustainability and overall process value of the system.[26,28,37,46,48–50] For example, Cu dispersed on titanium oxide nanorods was reported to be effective for the conversion of polyols and sugars into syngas and methanol under UV light irradiation and ambient conditions.[49] Decreased water content inhibited the formation of CO_2, whereas the copper loading amount controlled the decomposition way of the formic acid intermediate. Controlling the oxidation half-reaction is essential to produce

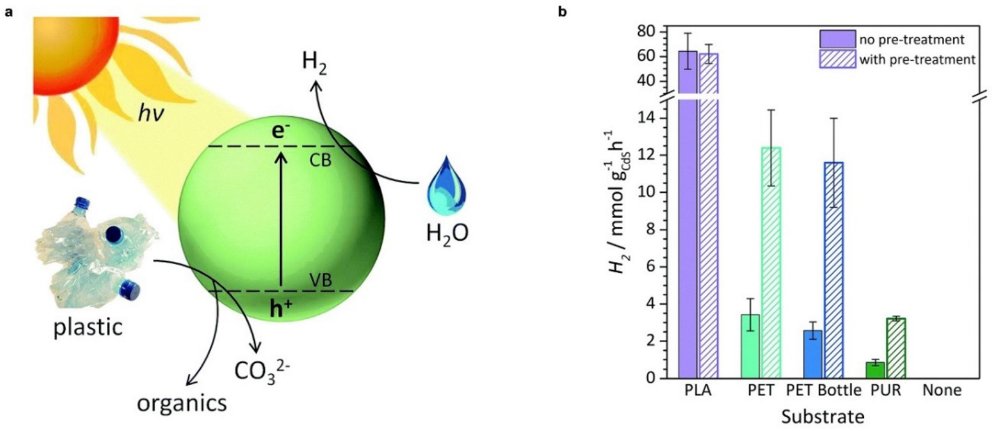

Fig. 3 (a) Diagram of the photoreforming of plastic waste using a CdS/CdO_x quantum dot photocatalyst. (b) Photoreforming of polymers to H_2 using CdS/CdO_x quantum dots under simulated solar light (AM 1.5G, 100 mW cm^{-2}). Reproduced with permission from ref. 37. Copyright 2018 The Royal Society of Chemistry.

high-value organic products instead of CO_2.[21,41] In addition, pre-treatment, including physical pre-treatment (such as crushing, shredding, and grinding) and chemical pre-treatment (such as hydrolysis and solubilization under highly alkaline or acidic conditions), is one of the most critical barriers to the practical application of the current photocatalytic reforming systems, adding significant cost and time to the overall process. Recently, it was demonstrated that metal salt hydrate solutions allowed for the complete solubilization of biomass and could be used as a reaction medium for the photocatalytic reforming of lignocellulose to produce H_2 and organic products under more benign conditions than the typically required extremely alkaline aqueous solutions, though the photocatalysts suffered from partial deactivation due to metal salt hydrate adsorption, necessitating future development.[50]

Organic transformation

Since the pioneering work of Kolbe that reported the electrochemical oxidation of organic molecules with the goal of developing new methods for synthesizing organic small molecules,[51] a larger body of research has grown around this topic in the ensuing decades. Over the past decade, photocatalytic processes that use light as the energy input have emerged as a new alternative approach in the repertoire of the organic synthesis toolbox. In particular, interest has been aroused in waste biomass valorization in order to produce high-value commodity chemicals instead of CO_2. Researchers have succeeded in converting biomass-derived small molecules such as 5-hydroxymethylfurfural (HMF) and furfural alcohol into higher-value materials (*e.g.*, aldehydes and acids) (Fig. 4a).[52–54] For example, photocatalytic H_2 evolution coupled with HMF (7110 $ per kg) oxidation to 2,5-diformylfuran (DFF) (198 000 $ per kg)[55] using porous carbon nitride was reported to reach a DFF yield of 13.8% with >99% selectivity after 6 h under visible light.[53]

Recent research has revealed a wide range of photocatalysts for oxidizing alcohols in conjunction with H_2 production.[57,58,62–65] Alcohols such as methanol have been widely used as sacrificial reagents for photocatalytic H_2 generation from water due to the lower thermodynamic requirements, and alcohols are oxidized to CO_2.[3–5] We will not discuss these examples because the focus of this work is on the co-production of high-value chemicals with H_2. For instance, under visible light irradiation, the coupling of H_2 generation with the oxidation of benzyl alcohol (273 $ per kg) yielded deoxybenzoin (57 200 $ per kg) over ZnIn sulfides,[55,58] and 4-methylbenzyl alcohol (2110 $ per kg) was converted into an aldehyde (4-methylbenzaldehyde; 3440 $ per kg) over a cyanamide surface functionalized with melon-type carbon nitride.[55,57] Multi-carbon alcohols and polyalcohols have been reported to be photocatalytically produced by selectively activating the inert sp^3 α-C–H bonds of alcohols and directly forming C–C bonds with the

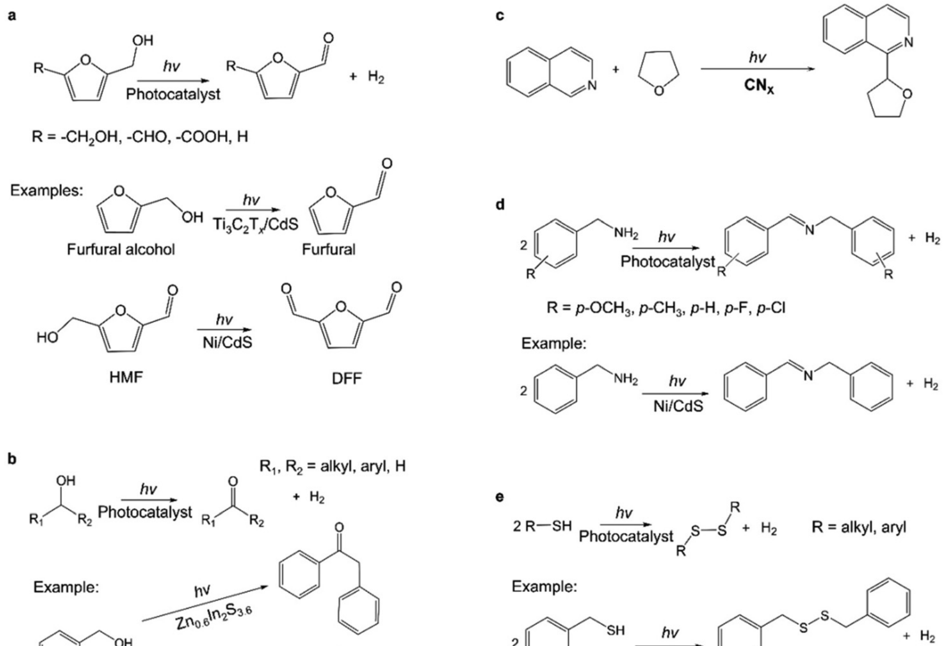

Fig. 4 (a) Photocatalytic oxidation of biomass-derived intermediate compounds.[52,54,56] HMF: 5-hydroxymethylfurfural; DFF: 2,5-diformylfuran. (b) Photocatalytic oxidation of alcohols.[57,58] (c) Photocatalytic Minisci coupling.[59] (d) Photocatalytic C–N coupling reactions.[56,60] (e) Photocatalytic S–S coupling reactions.[56,61]

coupling partners (Fig. 4b).[62] For instance, $Zn_2In_2S_5$ and CdS were reported as visible-light-responsive photocatalysts for the selective activation of the α-C–H bond of methanol to generate ethylene glycol with a selectivity of as high as 90%.[66,67] The CdS-based photocatalytic system was beneficial for the activation of the C–H bond in methanol without affecting the O–H group, forming ethylene glycol *via* a $^{\bullet}CH_2OH$ radical intermediate with a yield of 16% and a quantum efficiency (QE) of above 5.0% at wavelengths ≤450 nm.[66] The high ethylene glycol selectivity (90%) was maintained throughout the 100-hour reaction, with a yield of 16% after 100 hours, demonstrating an alternative nonpetroleum strategy for ethylene glycol synthesis. The $CoP/Zn_2In_2S_5$ photocatalyst also was demonstrated to be the first example of the visible-light-driven dehydrogenative coupling of ethanol to 2,3-butanediol with a selectivity of 53%.[67] The α-C–H bond of ethanol was selectively activated to form $^{\bullet}CH(OH)CH_3$ radicals for subsequent coupling to 2,3-butanediol, presenting that the α-C–H bond can be preferentially activated in the presence of the O–H group under mild conditions.

Aside from alcohols, the C–H bonds in furanics can also be activated for C–C coupling reactions through photocatalysis. The production of diesel fuel precursors from 2,5-dimethylfuran (2,5-DMF) and 2-methylfuran (2-MF), with concurrent H_2 production, over a Ru–$ZnIn_2S_4$ photocatalyst was demonstrated under visible light irradiation (Fig. 5).[68] Dehydrocoupling of

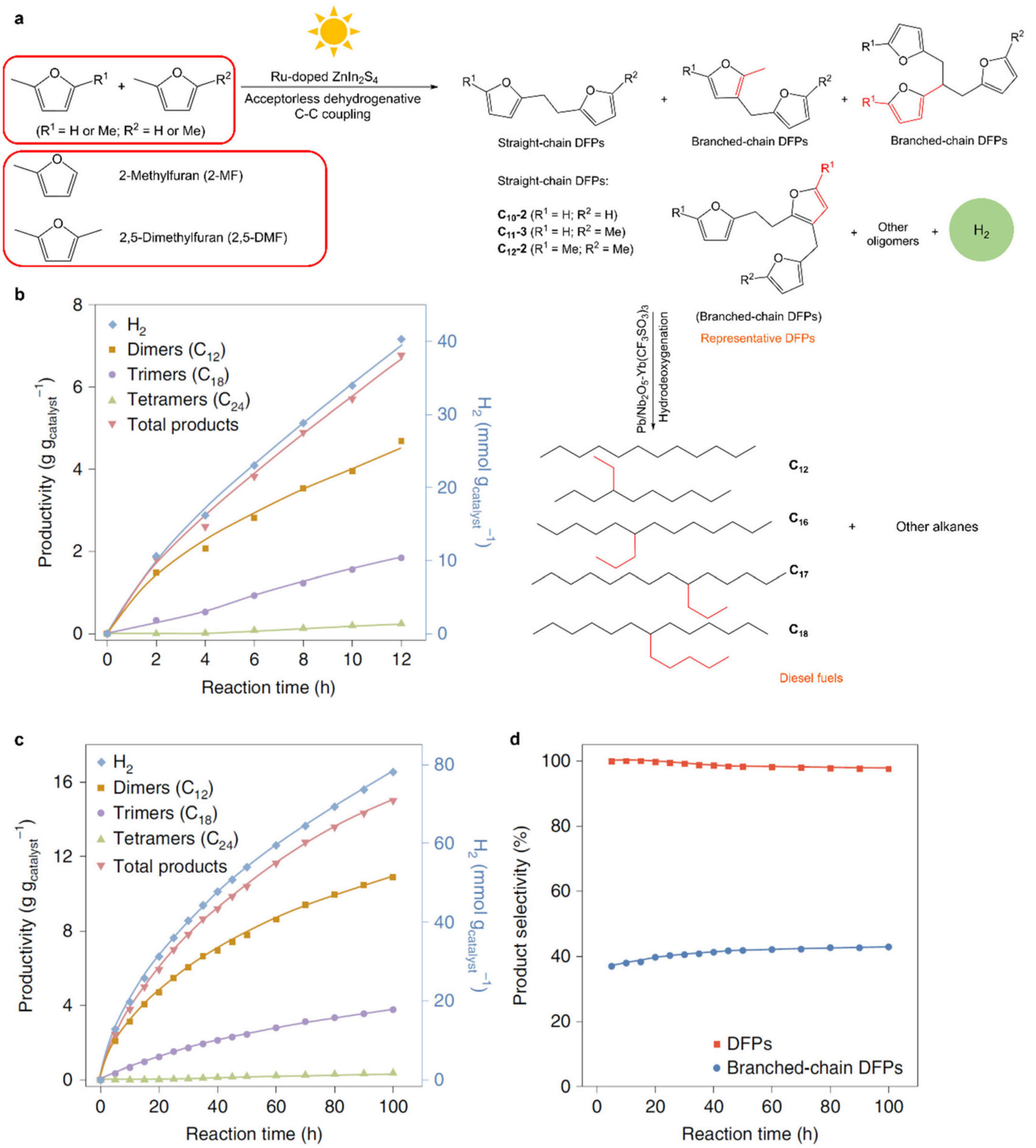

Fig. 5 (a) Schematic representation of the photocatalytic transformation of 2,5-DMF/2-MF into diesel fuel. (b–d) Photocatalytic dehydrocoupling of 2,5-DMF as a substrate: standard experiment (b), catalyst lifetime evaluation (c), and selectivity to oxygenated DFPs and branched-chain DFPs (d). Reproduced with permission from ref. 68. Copyright 2019 Springer Nature Limited.

2,5-DMF and 2-MF yielded mainly H_2, dimers and trimers as products with a small number of tetramers produced in 12 h. Photogenerated holes oxidized the furfuryl C–H bond of 2,5-DMF/2-MF, delivering protons and furfuryl radicals that, through C–C coupling, form the desired DFPs. Over Ru–$ZnIn_2S_4$, the QE for the dehydrocoupling of 2,5-DMF was 15.2% at 452 nm, which was approximately double that of $ZnIn_2S_4$ because Ru dopants substituted for indium ions in the $ZnIn_2S_4$ matrix facilitated charge separation efficiency and thus accelerated C–H activation. Diesel fuel precursors were produced with selectivities of more than 96% in conjunction with H_2 generation and were subsequently transformed into diesel fuels composed of straight- and branched-chain alkanes that were comparable to petroleum diesel in terms of alkane constituents. Future work should focus on improving the yields of C–C coupling products and the QE by the use of more efficient catalysts.

Lately, it has been demonstrated that H_2 production could be coupled with more complex organic synthesis. The Minisci reaction is a known strategy for the direct functionalization of C–H bonds in heteroarenes, involving the radical coupling of electron-deficient heteroarenes with oxidatively-generated nucleophilic radicals.[59] A visible light-mediated Minisci coupling of N-heteroarenes with ethers, alcohols, and amides in the presence of aerobic oxygen as an oxidant was reported to conjugate with proton reduction to H_2 using a cyanamide functionalized carbon nitride photocatalyst (Fig. 4c).[59]

Photocatalytic C–N coupling of amines for the efficient synthesis of imines may have important applications in pharmaceutical and agricultural chemistry research (Fig. 4d).[56] Ni/CdS was reported to photocatalyze the non-oxygen coupling of amines to yield their corresponding imines under visible light irradiation, concurrent with H_2 generation.[60,69] In particular, the photocatalyst showed a high conversion of benzylamine (99%) with 97% selectivity for imines, associated with a QE of 11.2% at 450 nm for simultaneous H_2 evolution.[60] By constructing *in situ* photoimmobilized Ni clusters on two-dimensional ultrathin CdS nanosheets, the generation of imines was dramatically improved with a QE of ~44% at 420 nm for the conversion of 4-methoxybenzylamine.[69] It was proposed that photogenerated holes initiated the oxidation of amines *via* the deprotonation process with the creation of C-centered α-amine radicals to form aldimine intermediates and release protons. The protons were reduced by the photogenerated electrons and produced H_2 with the assistance of a Ni cocatalyst. Additionally, the photocatalytic system converted a wide range of primary and secondary amines (*i.e.*, heterocyclic, aliphatic, and N-heterocycles) to form their corresponding imines with high yields (≥84%) and selectivity (≥95%), thereby offering a promising and versatile pathway for organic chemical synthesis.

The photocatalytic synthesis of disulfides through the coupling of thiols is also of interest because disulfides function as protecting groups in synthetic applications and as vulcanizing agents for rubber (Fig. 4e). One of the examples is the visible-light irradiation of CdSe quantum dots to result in virtually quantitative coupling of a variety of thiols, exemplified by 3-mercaptopropionic acid (MPA), to produce disulfides and H_2 in aqueous solution.[70] The conversion of MPA reached 99% in 1.5 hours and the yield of 3,3′-dithiodipropanoic acid was near 100%. Likewise, PtS/$ZnIn_2S_4$ completely transformed benzyl mercaptan to produce dibenzyl disulfide in 6 h with a selectivity of ~100% under optimal conditions.[61] These examples demonstrated an attractive alternative to existing procedures for synthesizing disulfides from thiols.

Controlling the selectivity of products is the most important issue of organic synthesis, as well as the existence of various potential reactive oxygen species in photocatalysis, including superoxide radicals ($^{\bullet}O_2^-$), hydrogen peroxide (H_2O_2), hydroxyl radicals ($^{\bullet}OH$) and singlet oxygen ($^1O_2$).[71] For selective oxidation, the reactive oxygen species and adsorption–desorption behavior must be carefully controlled.

Inorganic oxidation

Photocatalytic H_2 production along with more valuable inorganic products rather than O_2 *via* a two-electron oxidation pathway represents an alternatively appealing way. For instance, hydrogen peroxide (H_2O_2) production from water *via* the two-electron oxidation process is kinetically more favorable than the water-splitting reaction, which requires four electrons to produce O_2, despite the O_2 generation (1.23 eV *vs.* NHE) showing a thermodynamic advantage over the H_2O_2 production (1.78 eV *vs.* NHE). The photocatalytic reaction to simultaneously produce H_2 and H_2O_2 from water (eqn (11)) has attracted increasing attention in recent years because it obtains clean H_2 energy by utilizing abundant water resources and inexhaustible sunlight,[72,73] as well as being environmentally friendly for producing the value-added H_2O_2 (~0.7 $ per kg),[9] which was widely utilized in the chemical industry, and disinfection, energy, and environmental fields.[74–77] In addition, this reaction not only realizes the automatic separation of the oxidation product with gaseous H_2 but also effectively avoids the reverse reaction of generated H_2 and O_2 existing in the thoroughly overall water splitting reaction.[78,79]

$$2H_2O \rightarrow H_2 + H_2O_2 \tag{11}$$

Recent efforts, including optimizing reaction conditions, doping, heterojunctions, cocatalyst loading, and using biological hybrids, have been made to enhance the carrier utilization efficiency of the photocatalyst and increase the selectivity for H_2O_2 production, thereby advancing this technology. Graphitic carbon nitride (g-C_3N_4), for example, as a notable photocatalyst with advantageous features of low cost and tunable optical and electronic properties was widely employed in this field. A sulfur doping treatment was performed on thin g-C_3N_4 nanosheets to compensate for the light absorption loss caused by the exfoliation process while improving the charge transfer efficiency.[80] Moreover, Co_xNi_yP nanoclusters were loaded onto a P-doped g-C_3N_4 photocatalyst, and the doping and cocatalyst effects enhanced the photocatalytic water reduction and oxidation with a H_2 evolution rate of 239.3 μmol $g_{catalyst}^{-1}$ h^{-1} and stoichiometric H_2O_2 production.[81] It is also reported that the living *Chlorella* vulgaris could accelerate the photocatalytic activity of g-C_3N_4 to produce H_2O_2 and H_2 from water, giving a QE of 0.86% at 420 nm.[82] The defect control is also a proposed way applicable to increase H_2O_2 production. Although defects are typically regarded as charge recombination sites, it has been demonstrated that if properly controlled, they can also contribute to photocatalytic reactions.[83] Defects can introduce mid-gap states in the forbidden band of semiconductor photocatalysts to harness more visible light, serve as active sites for reactants, and offer more trapping sites to hamper the recombination of carriers.[84] For example, the introduced carbon vacancies in C_3N_4 can not only extend the light absorption range and improve carrier separation efficiency but also alter the H_2O_2 production pathway from a two-step indirect reaction to a one-step direct reaction, thereby enhancing the H_2O_2 production.[85] Construction of heterojunctions appears to be an effective strategy for inorganic semiconductor photocatalysts to generate H_2 and H_2O_2 simultaneously. For instance, a system consisting of CdS and $ZnIn_2S_4$ hollow cubes was employed for the stoichiometric generation of H_2 and H_2O_2 from pure water, achieving a QE of 1.63% at 400 nm.[86] Noble metal deposition remains a common but effective way to promote photocatalytic reactions. Production of H_2 and H_2O_2 with rates of 9.8 μmol $mg_{catalyst}^{-1}$ h^{-1} and 8.2 μmol $mg_{catalyst}^{-1}$ h^{-1}, respectively, from pure water (pH ~ 7) was realized using Pt/porous brookite TiO_2 nanoflutes as a photocatalyst, and the QE reached 43.4% at 365 nm.[87] The simulation and experimental results revealed that a two-electron reaction is kinetically favorable on the surface of brookite TiO_2 due to the unique surficial chemistry micro-circumstance, promoting the adsorption of activated hydroxyl groups and the subsequent step of hydrogen peroxide generation.

Though some promising progress has been made, photocatalytic H_2O_2 production is still far from the market requirement for practical applications, and the industrial production of H_2O_2 still mainly relies on the anthraquinone oxidation process (accounting for over 95% of production).[88] Facing the same problems with other semiconductor photocatalysis, photocatalytic H_2O_2 production also suffers from the drawbacks of low light utilization ability and the high recombination of photogenerated carriers. Another tricky problem is the rapid decomposition of the generated H_2O_2 occurs at the surface of the photocatalyst/cocatalyst, which can be caused by UV irradiation. More efforts should be devoted to the surface modification and fine control of the photocatalyst/cocatalyst and new cocatalyst development to promote H_2O_2 evolution and inhibit its decomposition process. For example, the combination of common inorganic semiconductor photocatalysts with bacteria, biomaterials, and organic semiconductors may have some positive effects. Additionally, a deeper understanding of the photocatalytic mechanism and H_2O_2 evolution process is significant and will contribute to the optimization and design of highly active photocatalysts.

$$2HX \rightarrow H_2 + X_2 \tag{12}$$

$$2Cl^- \rightarrow Cl_2 + 2e^- \quad E^\circ = +1.36\ V \tag{13}$$

$$2Br^- \rightarrow Br_2 + 2e^- \quad E^\circ = +1.09\ V \tag{14}$$

$$2I^- \rightarrow I_2 + 2e^- \quad E^\circ = +0.54\ V \tag{15}$$

Photocatalytic hydrohalic acid (HX, X = Cl^-, Br^-, I^-) splitting (eqn (12)) is another attractive approach for producing H_2 with a valuable byproduct X_2, which has numerous applications in the energy and hygiene industries.[89–91] Halide ion (Br^-, I^-) oxidation (eqn (13)–(15)) is thermodynamically much easier than H_2O oxidation, and more importantly, these photocatalytic reactions are conducted under the conditions of a relatively high H^+/X^- concentration, allowing for a faster reaction rate in dynamics. In addition, the oxidation of halide ions does not involve a net proton transfer, distinct from the H–O breakage and proton loss during O_2 formation in H_2O splitting, and thus are kinetically favorable. As an example, chloride oxidation catalyzed by silver ions in concentrated Cl^- solution has been reported, and the chloride complex-assisted catalysis mechanism has been proposed.[92] The research on chloride oxidation could promote the development of photocatalytic seawater splitting, which is still in its infancy due to its low product yield and a plausible catalytic mechanism involving the effect of inorganic ions, yet having been studied for years.[93,94]

Photocatalytic HBr and HI splitting to produce H_2 based on halide perovskites has aroused a new research upsurge in recent years since the first report about the hydrogen generation from hydriodic acid using $MAPbI_3$ as a photocatalyst in 2016 (Fig. 6a–c).[95] Subsequently, material compositing and heterojunction construction were extensively employed to boost hydrohalic acid splitting. Reduced graphene oxide (rGO) was first used to composite with $MAPbI_3$ perovskites for the photocatalytic hydrogen evolution reaction, resulting in a hydrogen evolution rate (93.9 μmol h^{-1} under visible-light irradiation) 67 times higher than that of pure $MAPbI_3$.[96] Afterwards, various materials such as TiO_2, Ni_3C, carbon dots, black phosphorus, MoS_2, and CoP were used as cocatalysts or heterojunction counterparts to promote carrier separation.[97–103] In particular, a $MoS_2/MAPbI_3$ composite exhibited a remarkable photocatalytic hydrogen evolution activity of 29.4 μmol $g_{catalyst}^{-1}$ h^{-1} under visible light and an H_2 production of 103 mL day^{-1} under outdoor natural sunlight irradiation.[103] In addition to the heterostructures, composition regulation is also a feasible way. For instance, a graded and gradient halide ion distribution was realized in both organometal and all-inorganic mixed halide perovskites,[104,105] and a resulting bandgap funneling was constructed for efficient carrier transfer, causing an enhanced photocatalytic activity and a solar-to-H_2 conversion efficiency (STH) of 1.05% for $MAPbBr_{3-x}I_x$/Pt.[104] In addition, single-atom decoration is also an effective strategy to improve the perovskite photocatalytic HI splitting efficiency,[106,107] an excellent photocatalytic H_2

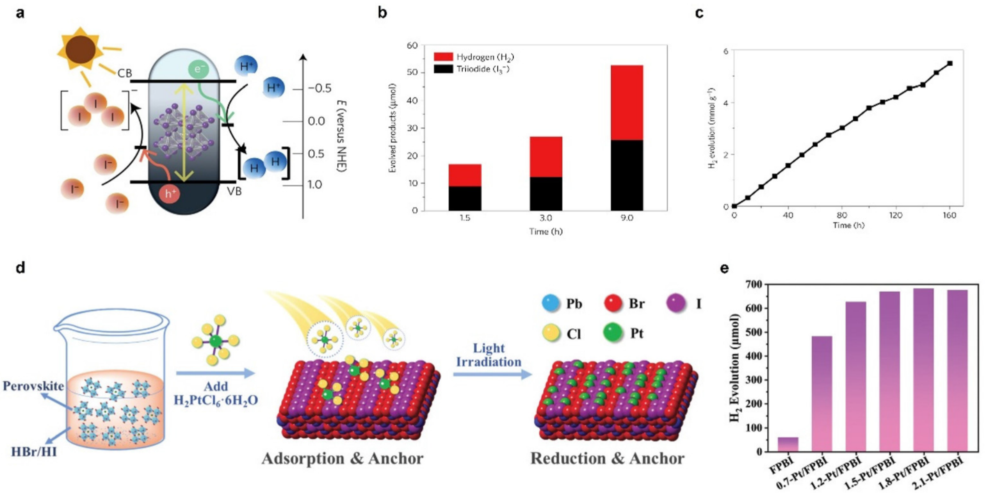

Fig. 6 (a) Schematic band diagram of $MAPbI_3$ powder for the HI splitting photocatalytic reaction. (b) Quantitative comparison between the evolved H_2 and I_3^-. (c) Stable photocatalytic H_2 evolution produced by $MAPbI_3$ powder in the saturated solution for 160 h (H_3PO_2 was added to the HI solution). Reproduced with permission from ref. 95. Copyright 2016 Springer Nature Limited. (d) Mechanism illustration of the synthesis process of Pt/$FAPbBr_{3-x}I_x$. (e) Photocatalytic H_2 evolution activities of ω-FPBI ($FAPbBr_{3-x}I_x$ loaded ω% Pt in mass percentage). Reproduced with permission from ref. 107. Copyright 2022 The Royal Society of Chemistry.

evolution rate of 682.6 mmol h^{-1} under simulated sunlight irradiation (area of π cm) and a corresponding STH of 4.5% were recorded using Pt/$FAPbBr_{3-x}I_x$ (Fig. 6d and e).[107]

Halide perovskites possess several excellent material properties, such as a wide light absorption range, a high absorption coefficient, and a long carrier diffusion length, allowing them to be ideal photocatalysts. However, satisfactory performance of this kind of material for photocatalytic H_2 production has not been achieved. More efforts should be devoted to the investigation of the mechanism and fundamental principles of the physical/chemical process during photocatalysis for this special system, where exists a dynamic equilibrium of dissolution-crystallization between the catalyst and the corresponding saturated solution.

Conclusions and outlook

Although the research in this field is at too early a stage to be towards industry-level operation and deployment, exciting work in combining H_2 fuel generation with value-added chemical production or waste valorization is already showing to have a wide impact on large-scale challenges in global energy (Table 1). When looking at both inorganic and organic chemistries, the water-to-O_2 conversion can be replaced by a variety of photoreactions that can occur in an aqueous solution.

In any proton-to-H_2 generation, the availability of substrates at the scale required for the process is a key consideration. Biomass, food, and plastic wastes are abundant, inexpensive, and carbon- and hydrogen-rich feedstocks. Photocatalytic methods offer upcycling routes that yield higher-value products, as opposed to conventional mechanical strategies that typically downcycle to lower-quality products.[11,40] In recent years, much effort has been devoted to the study of the simultaneous production of H_2 and chemicals with added value through reduction and oxidation, respectively. A preliminary techno-economic assessment demonstrates that photoreforming of waste can become economically competitive with existing technologies if the efficiency and lifetime can be substantially improved.[11] For large-scale applications to be economically and environmentally viable, H_2 evolution rates must increase by a factor of at least 50 (rates of >0.004 mol H_2 $g_{substrate}{}^{-1}$ h^{-1}, conversions of >50% per day, and QEs of >50%). It will be imperative to develop more effective and durable photocatalytic systems. In addition, the current pretreatments commonly reported for photoreforming to improve the solubilization of the feedstock are unlikely to be economically viable on a large scale.

The photocatalytic oxidation of organic compounds, including alcohols, hydrocarbons, aromatics, and amines, differs from conventional methods conducted at high temperatures and pressures in that it is environmentally friendly, operates under mild conditions, and is sustainable. However, selective photocatalytic oxidations present huge challenges. Ideally, the oxidation process would selectively produce a single high-value product. Controlling reactive oxidation species and adsorption–desorption behavior is the primary challenge in selective oxidation. Therefore, it may be necessary to observe the reaction mechanism *in situ* for a better understanding of the reaction kinetics.[71] To yield a single higher-value product in both organic transformation and waste valorization processes, selective oxidation cocatalysts may be required.

For inorganic reactions, the H_2O-to-H_2O_2 conversion and halide oxidation present themselves as an attractive alternative to O_2 evolution due to the higher value of the products and the simpler mechanism resulting from the lower electron demand.

Table 2 Summary of the developed alternative photooxidation reactions to the OER

Oxidation reaction	Substrates	Main products	Challenges
Reforming	Lignocellulose biomass-derived feedstocks (pentoses, hexoses, alcohols, and organic acids)	CO_2	• Costly and inefficient lignocellulose refining processes required • Low-value products
	Cellulose, hemicellulose, and lignin	CO_2	• Low substrate solubility • Low-value products
	Raw biomass	CO_2	• Low substrate solubility • Costly and environmentally unfriendly pre-treatment processes required • Low-value products
	Waste streams (biomass, food, and plastic)	CO_2, formate	• Low substrate solubility • Costly and environmentally unfriendly pre-treatment processes required • Competition with water reduction and plastic dehydrogenation to H_2
Organics	Alcohols		• Low selectivity
	Furans	Dimers and trimers	• Low selectivity
	Amines	Imine	
	Thiols	Disulfides	
Inorganics	Water	H_2O_2	
	HX (X = Cl^-, Br^-, I^-)	X_2	

Nonetheless, the reaction efficiency of these reactions must be enhanced.

The H_2 production cost for a waste photoreforming pilot plant (400 m^2, 200 kg_{waste} per day, 14.4 kg_{H_2} per day) was estimated to be £11.80 per kg, which is more than H_2 sale targets of £3–5 per kg and predictions for H_2 produced by photocatalytic water splitting (£1–3 per kg).[1,11] It can, however, be reduced by increasing the plant scale and photoreforming efficiency. If the plant scale is enlarged 30 times, the cost of producing H_2 can be decreased to £3 per kg. Furthermore, economic gains can be realized by producing high-value compounds such as pharmaceutical components at the same time. As an example, oxidizing biomass to 3-hydroxybutyrolactone (3-HBL), a precursor for chiral drugs, could cut H_2 production costs to £3 per kg even if the photoreforming conversion efficiency is as low as 0.2% per day. However, although 3-HBL and its hydrolyzed form 3,4-dihydroxybutyric acid (3,4-DHBA) have been reported to be produced from biomass (glucose, glycolic acid, and xylose) *via* biological synthesis using bacteria (*Escherichia coli*), enzymes and yeast, its production *via* a photocatalytic process has not yet been realized.[110–112] Future efforts would combine photocatalysts with microbes to create abiotic–biotic hybrids capable of producing photocatalytic H_2 while oxidizing biomass to 3-HBL. Likewise, the H_2 production costs can be reduced by photocatalytic transformations to produce value-added organic and inorganic chemicals. For instance, a recent techno-economic analysis suggested that by oxidizing water to produce H_2O_2 instead of O_2 using the photoelectrochemical technique, a levelized cost of hydrogen of \$6.19 per kg can be obtained with an STH of 10.1% and an H_2O_2 price of \$0.85 per kg, which is a significant improvement over the values found in an analogy of the photoelectrochemical water splitting system.[113] Aside from producing cost-effective H_2, the procedures would also reduce the cost of organic and inorganic products. A minimal selling price of glucaric acid was predicted to be \$6.94 per kg under a base case scenario employing a potential photo-biorefinery approach for sunlight-driven electro-oxidation of glucose, which was 70% lower than the current market price.[114]

In spite of the obstacles listed in Table 2, significant progress has been made in the study of coupling H_2 production with diverse oxidation chemistry and will continue. With continued material and technological advancements, these technologies have the potential to produce fuels and chemicals with added value, while also reducing waste.

Conflicts of interest

There are no conflicts to declare.

Acknowledgements

This work was supported by the JSPS Leading Initiative for Excellent Young Researchers Program (to Q. W.), the JST Fusion Oriented REsearch for Disruptive Science and Technology Program (no. 21470281, to Q. W.), and the JSPS Grant-in-Aid for Young Scientists (Start-up) (no. 21K20485; to Q. W.).

References

1 Q. Wang and K. Domen, *Chem. Rev.*, 2020, **120**, 919–985.
2 H. Inoue, T. Shimada, Y. Kou, Y. Nabetani, D. Masui, S. Takagi and H. Tachibana, *ChemSusChem*, 2011, **4**, 173–179.
3 X. Chen, S. Shen, L. Guo and S. S. Mao, *Chem. Rev.*, 2010, **110**, 6503–6570.

4 K. Zhang and L. Guo, *Catal. Sci. Technol.*, 2013, **3**, 1672–1690.

5 Y. Xu, Y. Huang and B. Zhang, *Inorg. Chem. Front.*, 2016, **3**, 591–615.

6 C. R. Lhermitte and K. Sivula, *ACS Catal.*, 2019, **9**, 2007–2017.

7 A. Y. Ru Ng, B. Boruah, K. F. Chin, J. M. Modak and H. S. Soo, *ChemNanoMat*, 2020, **6**, 185–203.

8 V. Andrei, Q. Wang, T. Uekert, S. Bhattacharjee and E. Reisner, *Acc. Chem. Res.*, 2022, **55**, 3376–3386.

9 . ChemAnalyst, **https://www.chemanalyst.com**, (accessed February 10, 2023).

10 L. M. Reid, T. Li, Y. Cao and C. P. Berlinguette, *Sustainable Energy Fuels*, 2018, **2**, 1905–1927.

11 T. Uekert, C. M. Pichler, T. Schubert and E. Reisner, *Nat. Sustain.*, 2021, **4**, 383–391.

12 M. F. Kuehnel and E. Reisner, *Angew. Chem., Int. Ed.*, 2018, **57**, 3290–3296.

13 D. I. Kondarides, V. M. Daskalaki, A. Patsoura and X. E. Verykios, *Catal. Lett.*, 2008, **122**, 26–32.

14 M. R. St. John, A. J. Furgala and A. F. Sammells, *J. Phys. Chem.*, 1983, **87**, 801–805.

15 H. Bahruji, M. Bowker, P. R. Davies, L. S. Al-Mazroai, A. Dickinson, J. Greaves, D. James, L. Millard and F. Pedrono, *J. Photochem. Photobiol., A*, 2010, **216**, 115–118.

16 T. Shiragami, T. Tomo, H. Tsumagari, R. Yuki, T. Yamashita and M. Yasuda, *Chem. Lett.*, 2012, **41**, 29–31.

17 Q. Xu, Y. Ma, J. Zhang, X. Wang, Z. Feng and C. Li, *J. Catal.*, 2011, **278**, 329–335.

18 Y. Li, D. Gao, S. Peng, G. Lu and S. Li, *Int. J. Hydrogen Energy*, 2011, **36**, 4291–4297.

19 R. Su, R. Tiruvalam, A. J. Logsdail, Q. He, C. A. Downing, M. T. Jensen, N. Dimitratos, L. Kesavan, P. P. Wells, R. Bechstein, H. H. Jensen, S. Wendt, C. R. A. Catlow, C. J. Kiely, G. J. Hutchings and F. Besenbacher, *ACS Nano*, 2014, **8**, 3490–3497.

20 A. V. Puga, *Coord. Chem. Rev.*, 2016, **315**, 1–66.

21 W. Deng, H. Zhang, L. Xue, Q. Zhang and Y. Wang, *Chin. J. Catal.*, 2015, **36**, 1440–1460.

22 X. Wu, N. Luo, S. Xie, H. Zhang, Q. Zhang, F. Wang and Y. Wang, *Chem. Soc. Rev.*, 2020, **49**, 6198–6223.

23 T. Kawai and T. Sakata, *Nature*, 1980, **286**, 474–476.

24 D. W. Wakerley, M. F. Kuehnel, K. L. Orchard, K. H. Ly, T. E. Rosser and E. Reisner, *Nat. Energy*, 2017, **2**, 17021.

25 L. Lan, H. Chen, D. Lee, S. Xu, N. Skillen, A. Tedstone, P. Robertson, A. Garforth, H. Daly, C. Hardacre and X. Fan, *ACS Sustainable Chem. Eng.*, 2022, **10**, 4862–4871.

26 D. S. Achilleos, W. Yang, H. Kasap, A. Savateev, Y. Markushyna, J. R. Durrant and E. Reisner, *Angew. Chem., Int. Ed.*, 2020, **59**, 18184–18188.

27 Q. Cheng, Y.-J. Yuan, R. Tang, Q.-Y. Liu, L. Bao, P. Wang, J. Zhong, Z. Zhao, Z.-T. Yu and Z. Zou, *ACS Catal.*, 2022, **12**, 2118–2125.

28 E. Wang, A. Mahmood, S.-G. Chen, W. Sun, T. Muhmood, X. Yang and Z. Chen, *ACS Catal.*, 2022, **12**, 11206–11215.

29 H. Kasap, D. S. Achilleos, A. Huang and E. Reisner, *J. Am. Chem. Soc.*, 2018, **140**, 11604–11607.

30 C. Rao, M. Xie, S. Liu, R. Chen, H. Su, L. Zhou, Y. Pang, H. Lou and X. Qiu, *ACS Appl. Mater. Interfaces*, 2021, **13**, 44243–44253.

31 S. R. Kadam, V. R. Mate, R. P. Panmand, L. K. Nikam, M. V. Kulkarni, R. S. Sonawane and B. B. Kale, *RSC Adv.*, 2014, **4**, 60626–60635.

32 C. Li, H. Wang, S. B. Naghadeh, J. Z. Zhang and P. Fang, *Appl. Catal.*, 2018, **227**, 229–239.

33 N. Skillen, H. Daly, L. Lan, M. Aljohani, C. W. J. Murnaghan, X. Fan, C. Hardacre, G. N. Sheldrake and P. K. J. Robertson, *Top. Curr. Chem.*, 2022, **380**, 33.

34 A. Speltini, M. Sturini, D. Dondi, E. Annovazzi, F. Maraschi, V. Caratto, A. Profumo and A. Buttafava, *Photochem. Photobiol. Sci.*, 2014, **13**, 1410–1419.

35 J. Zou, G. Zhang and X. Xu, *Appl. Catal., A*, 2018, **563**, 73–79.

36 K. Tomoji and S. Tadayoshi, *Chem. Lett.*, 1981, **10**, 81–84.

37 T. Uekert, M. F. Kuehnel, D. W. Wakerley and E. Reisner, *Energy Environ. Sci.*, 2018, **11**, 2853–2857.

38 C. M. Pichler, S. Bhattacharjee, M. Rahaman, T. Uekert and E. Reisner, *ACS Catal.*, 2021, **11**, 9159–9167.

39 T. Uekert, M. A. Bajada, T. Schubert, C. M. Pichler and E. Reisner, *ChemSusChem*, 2021, **14**, 4190–4197.

40 S. Chu, B. Zhang, X. Zhao, H. S. Soo, F. Wang, R. Xiao and H. Zhang, *Adv. Energy Mater.*, 2022, **12**, 2200435.

41 C. M. Pichler, S. Bhattacharjee, E. Lam, L. Su, A. Collauto, M. M. Roessler, S. J. Cobb, V. M. Badiani, M. Rahaman and E. Reisner, *ACS Catal.*, 2022, **12**, 13360–13371.

42 M. Han, S. Zhu, C. Xia and B. Yang, *Appl. Catal., B*, 2022, **316**, 121662.

43 Y. Li, S. Wan, C. Lin, Y. Gao, Y. Lu, L. Wang and K. Zhang, *Sol. RRL*, 2021, **5**, 2000427.

44 B. Cao, S. Wan, Y. Wang, H. Guo, M. Ou and Q. Zhong, *J. Colloid Interface Sci.*, 2022, **605**, 311–319.

45 T. Uekert, F. Dorchies, C. M. Pichler and E. Reisner, *Green Chem.*, 2020, **22**, 3262–3271.

46 T. Uekert, H. Kasap and E. Reisner, *J. Am. Chem. Soc.*, 2019, **141**, 15201–15210.

47 K. Su, H. Liu, C. Zhang and F. Wang, *Chin. J. Catal.*, 2022, **43**, 589–594.

48 E. Lam and E. Reisner, *Angew. Chem., Int. Ed.*, 2021, **60**, 23306.

49 M. Wang, M. Liu, J. Lu and F. Wang, *Nat. Commun.*, 2020, **11**, 1083.

50 C. M. Pichler, T. Uekert and E. Reisner, *Chem. Commun.*, 2020, **56**, 5743–5746.

51 H. Kolbe, *Justus Liebigs Ann. Chem.*, 1849, **69**, 257–294.

52 G. Han, Y.-H. Jin, R. A. Burgess, N. E. Dickenson, X.-M. Cao and Y. Sun, *J. Am. Chem. Soc.*, 2017, **139**, 15584–15587.

53 V. R. Battula, A. Jaryal and K. Kailasam, *J. Mater. Chem. A*, 2019, **7**, 5643–5649.

54 Y.-H. Li, F. Zhang, Y. Chen, J.-Y. Li and Y.-J. Xu, *Green Chem.*, 2020, **22**, 163–169.

55 MilliporeSigma, https://www.sigmaaldrich.com/US/en, (accessed February 10, 2023).

56 J.-H. Tang and Y. Sun, *Mater. Adv.*, 2020, **1**, 2155–2162.

57 H. Kasap, C. A. Caputo, B. C. M. Martindale, R. Godin, V. W.-h. Lau, B. V. Lotsch, J. R. Durrant and E. Reisner, *J. Am. Chem. Soc.*, 2016, **138**, 9183–9192.

58 N. Luo, T. Hou, S. Liu, B. Zeng, J. Lu, J. Zhang, H. Li and F. Wang, *ACS Catal.*, 2020, **10**, 762–769.

59 A. Vijeta and E. Reisner, *Chem. Commun.*, 2019, **55**, 14007–14010.

60 W. Yu, D. Zhang, X. Guo, C. Song and Z. Zhao, *Catal. Sci. Technol.*, 2018, **8**, 5148–5154.

61 L. Xu, X. Deng and Z. Li, *Appl. Catal., B*, 2018, **234**, 50–55.

62 Z. Gao, N. Luo, Z. Huang, S. H. Taylor and F. Wang, *ACS Sustainable Chem. Eng.*, 2021, **9**, 6188–6202.

63 D. Antón-García, E. Edwardes Moore, M. A. Bajada, A. Eisenschmidt, A. R. Oliveira, I. A. C. Pereira, J. Warnan and E. Reisner, *Nat. Synth.*, 2022, **1**, 77–86.

64 X. Ye, Y. Chen, Y. Wu, X. Zhang, X. Wang and S. Chen, *Appl. Catal., B*, 2019, **242**, 302–311.

65 F. Li, Y. Wang, J. Du, Y. Zhu, C. Xu and L. Sun, *Appl. Catal., B*, 2018, **225**, 258–263.

66 S. Xie, Z. Shen, J. Deng, P. Guo, Q. Zhang, H. Zhang, C. Ma, Z. Jiang, J. Cheng, D. Deng and Y. Wang, *Nat. Commun.*, 2018, **9**, 1181.

67 H. Zhang, S. Xie, J. Hu, X. Wu, Q. Zhang, J. Cheng and Y. Wang, *Chem. Commun.*, 2020, **56**, 1776–1779.

68 N. Luo, T. Montini, J. Zhang, P. Fornasiero, E. Fonda, T. Hou, W. Nie, J. Lu, J. Liu, M. Heggen, L. Lin, C. Ma, M. Wang, F. Fan, S. Jin and F. Wang, *Nat. Energy*, 2019, **4**, 575–584.

69 Y. Huang, C. Liu, M. Li, H. Li, Y. Li, R. Su and B. J. A. C. Zhang, *ACS Catal.*, 2020, **10**, 3904–3910.

70 X. B. Li, Z. J. Li, Y. J. Gao, Q. Y. Meng, S. Yu, R. G. Weiss, C. H. Tung and L. Z. Wu, *Angew. Chem., Int. Ed.*, 2014, **126**, 2117–2121.

71 L. Xiong and J. Tang, *Adv. Energy Mater.*, 2021, **11**, 2003216.

72 Y. F. Zhang and S. J. Park, *J. Mater. Chem. A*, 2018, **6**, 20304–20312.

73 J. Chen, N. Kang, J. Fan, C. Lu and K. Lv, *Mater. Today Chem.*, 2022, **26**, 101028.

74 K. P. Bryliakov, *Chem. Rev.*, 2017, **117**, 11406–11459.

75 Z. Tang, P. Zhao, H. Wang, Y. Liu and W. Bu, *Chem. Rev.*, 2021, **121**, 1981–2019.

76 J. Xu, X. Zheng, Z. Feng, Z. Lu, Z. Zhang, W. Huang, Y. Li, D. Vuckovic, Y. Li, S. Dai, G. Chen, K. Wang, H. Wang, J. K. Chen, W. Mitch and Y. Cui, *Nat. Sustain.*, 2021, **4**, 233–241.

77 J. Y. Tang, T. S. Zhao, D. Solanki, X. B. Miao, W. G. Zhou and S. Hu, *Joule*, 2021, **5**, 1432–1461.

78 K. Li, M. Han, R. Chen, S. L. Li, S. L. Xie, C. Mao, X. Bu, X. L. Cao, L. Z. Dong, P. Feng and Y. Q. Lan, *Adv. Mater.*, 2016, **28**, 8906–8911.

79 R. Shi, H.-F. Ye, F. Liang, Z. Wang, K. Li, Y. Weng, Z. Lin, W.-F. Fu, C.-M. Che and Y. Chen, *Adv. Mater.*, 2018, **30**, 1705941.

80 C. Feng, L. Tang, Y. Deng, J. Wang, Y. Liu, X. Ouyang, H. Yang, J. Yu and J. Wang, *Appl. Catal., B*, 2021, **281**, 119539.

81 F. Xue, Y. Si, M. Wang, M. Liu and L. Guo, *Nano Energy*, 2019, **62**, 823–831.

82 Y. Fu, C. a. Liu, M. Zhang, C. Zhu, H. Li, H. Wang, Y. Song, H. Huang, Y. Liu and Z. Kang, *Adv. Energy Mater.*, 2018, **8**, 1802525.

83 Z. Pei, L. Ding, J. Hu, S. Weng, Z. Zheng, M. Huang and P. Liu, *Appl. Catal., B*, 2013, **142–143**, 736–743.

84 H. Hou, X. Zeng and X. Zhang, *Angew. Chem., Int. Ed.*, 2020, **59**, 17356–17376.

85 S. Li, G. Dong, R. Hailili, L. Yang, Y. Li, F. Wang, Y. Zeng and C. Wang, *Appl. Catal., B*, 2016, **190**, 26–35.

86 E. Zhang, Q. Zhu, J. Huang, J. Liu, G. Tan, C. Sun, T. Li, S. Liu, Y. Li, H. Wang, X. Wan, Z. Wen, F. Fan, J. Zhang and K. Ariga, *Appl. Catal., B*, 2021, **293**, 120213.

87 S. Cao, T.-S. Chan, Y.-R. Lu, X. Shi, B. Fu, Z. Wu, H. Li, K. Liu, S. Alzuabi, P. Cheng, M. Liu, T. Li, X. Chen and L. Piao, *Nano Energy*, 2020, **67**, 104287.

88 J. M. Campos-Martin, G. Blanco-Brieva and J. L. G. Fierro, *Angew. Chem., Int. Ed.*, 2006, **45**, 6962–6984.

89 B. Huskinson, J. Rugolo, S. K. Mondal and M. J. Aziz, *Energy Environ. Sci.*, 2012, **5**, 8690–8698.

90 G. R. Taylor and M. Butler, *Epidemiol. Infect.*, 1982, **89**, 321–328.

91 R. Yeo and D. T. Chin, *J. Electrochem. Soc.*, 1980, **127**, 549.

92 J. Du, Z. Chen, C. Chen and T. J. Meyer, *J. Am. Chem. Soc.*, 2015, **137**, 3193–3196.

93 Y. Wang, L. Shi, H. Hu, *et al.*, Binary trinuclear metal-oxo sub-nanomaterials for photocatalytic hydrogen and chlorine production from seawater, *SusMat*, 2022, **2**, 708–719.

94 J. Zhang, Y. Lei, S. Cao, W. Hu, L. Piao and X. Chen, *Nano Res.*, 2022, **15**, 2013–2022.

95 S. Park, W. J. Chang, C. W. Lee, S. Park, H.-Y. Ahn and K. T. Nam, *Nat. Energy*, 2016, **2**, 16185.

96 Y. Wu, P. Wang, X. Zhu, Q. Zhang, Z. Wang, Y. Liu, G. Zou, Y. Dai, M.-H. Whangbo and B. Huang, *Adv. Mater.*, 2018, **30**, 1704342.

97 C. Cai, Y. Teng, J.-H. Wu, J.-Y. Li, H.-Y. Chen, J.-H. Chen and D.-B. Kuang, *Adv. Funct. Mater.*, 2020, **30**, 2001478.

98 Z. Zhao, J. Wu, Y.-Z. Zheng, N. Li, X. Li and X. Tao, *ACS Catal.*, 2019, **9**, 8144–8152.

99 X. Wang, H. Wang, H. Zhang, W. Yu, X. Wang, Y. Zhao, X. Zong and C. Li, *ACS Energy Lett.*, 2018, **3**, 1159–1164.

100 R. Li, X. Li, J. Wu, X. Lv, Y.-Z. Zheng, Z. Zhao, X. Ding, X. Tao and J.-F. Chen, *Appl. Catal., B*, 2019, **259**, 118075.

101 Y. Zhao, Q. Zeng, Y. Yu, T. Feng, Y. Zhao, Z. Wang, Y. Li, C. Liu, J. Liu, H. Wei, S. Zhu, Z. Kang, H. Zhang and B. Yang, *Mater. Horiz.*, 2020, **7**, 2719–2725.

102 W. Guan, Y. Li, Q. Zhong, H. Liu, J. Chen, H. Hu, K. Lv, J. Gong, Y. Xu, Z. Kang, M. Cao and Q. Zhang, *Nano Lett.*, 2021, **21**, 597–604.

103 X. L. Zhao, S. Chen, H. J. Yin, S. Y. Jiang, K. Zhao, J. Kang, P. F. Liu, L. X. Jiang, Z. J. Zhu, D. D. Cui, P. R. Liu,

X. J. Han, H. G. Yang and H. J. Zhao, *Matter*, 2020, **3**, 935–949.

104 Y. Wu, P. Wang, Z. Guan, J. Liu, Z. Wang, Z. Zheng, S. Jin, Y. Dai, M.-H. Whangbo and B. Huang, *ACS Catal.*, 2018, **8**, 10349–10357.

105 Z. Guan, Y. Wu, P. Wang, Q. Zhang, Z. Wang, Z. Zheng, Y. Liu, Y. Dai, M.-H. Whangbo and B. Huang, *Appl. Catal., B*, 2019, **245**, 522–527.

106 P. Zhou, H. Chen, Y. Chao, Q. Zhang, W. Zhang, F. Lv, L. Gu, Q. Zhao, N. Wang, J. Wang and S. Guo, *Nat. Commun.*, 2021, **12**, 4412.

107 Y. Wu, Q. Wu, Q. Zhang, Z. Lou, K. Liu, Y. Ma, Z. Wang, Z. Zheng, H. Cheng, Y. Liu, Y. Dai, B. Huang and P. Wang, *Energy Environ. Sci.*, 2022, **15**, 1271–1281.

108 V.-C. Nguyen, D. B. Nimbalkar, L. D. Nam, Y.-L. Lee and H. Teng, *ACS Catal.*, 2021, **11**, 4955–4967.

109 H. Li, Z. Gao, L. Lei, H. Liu, J. Han, F. Hong, N. Luo and F. Wang, *Green Chem.*, 2020, **22**, 3802–3808.

110 T. Yukawa, T. Bamba, M. Matsuda, T. Yoshida, K. Inokuma, J. Kim, J. Won Lee, Y.-S. Jin, A. Kondo and T. Hasunuma, *Biotechnol. Bioeng.*, 2023, **120**, 511–523.

111 C. H. Martin, H. Dhamankar, H.-C. Tseng, M. J. Sheppard, C. R. Reisch and K. L. J. Prather, *Nat. Commun.*, 2013, **4**, 1414.

112 H. Dhamankar, Y. Tarasova, C. H. Martin and K. L. J. Prather, *Metab. Eng.*, 2014, **25**, 72–81.

113 K. Wenderich, W. Kwak, A. Grimm, G. J. Kramer, G. Mul and B. Mei, *Sustainable Energy Fuels*, 2020, **4**, 3143–3156.

114 M. A. Khan, T. A. Al-Attas, N. G. Yasri, H. Zhao, S. Larter, J. Hu and M. G. Kibria, *Sustainable Energy Fuels*, 2020, **4**, 5568–5577.